Numerical Modelling of a Lightning Strike on a Protected Composite Panel

Christine Espinosa, H. Bhoosnurmath, A. Carcel Lopez, Frederic Lachaud

▶ **To cite this version:**

Christine Espinosa, H. Bhoosnurmath, A. Carcel Lopez, Frederic Lachaud. Numerical Modelling of a Lightning Strike on a Protected Composite Panel. ICOLSE 2017 International Conference on Lightning and Static Electricity, 13-15 sept. 2017, Nagoya (J), Sep 2017, Nagoya, Japan. hal-02044384

HAL Id: hal-02044384
https://hal.science/hal-02044384v1

Submitted on 19 Feb 2025

HAL is a multi-disciplinary open access archive for the deposit and dissemination of scientific research documents, whether they are published or not. The documents may come from teaching and research institutions in France or abroad, or from public or private research centers.

L'archive ouverte pluridisciplinaire **HAL**, est destinée au dépôt et à la diffusion de documents scientifiques de niveau recherche, publiés ou non, émanant des établissements d'enseignement et de recherche français ou étrangers, des laboratoires publics ou privés.

Numerical Modelling of a Lightning Strike on a Protected Composite Panel

C Espinosa*, H Bhoosnurmath†, A C López†, F Lachaud*

* *Institut Clément Ader (ICA), Université de Toulouse, CNRS-INSA-ISAE-Mines Albi-UPS,*
3 Rue Caroline Aigle, 31077 Toulouse Cedex 4, France
† *Institut Supérieur de l'Aéronautique et de l'Espace (ISAE-Supaero),10 Avenue E. Belin, 31400 Toulouse, France*
christine.espinosa@isae-supaero.fr

Keywords: lightning strike, composite panel delamination, solid copper foil, coupled thermal-mechanical, FEM

Abstract

The increased usage of carbon-fibre reinforced polymer (CFRP) composites in aerospace has made the investigation of the *direct effects* of a lightning strike (LS) on protected CFRP desirable. Among others, recent works based on the electrical-thermal model of Ogasawara et al. [1] use electrical-thermal analysis to evaluate the effect of resin pyrolysis on the induced bulk damage of unprotected CFRP panels [2]. A coupled thermal-mechanical model is proposed here which considers non-linearities and temperature dependency of material behaviour for the lightning strike protection (LSP) and CFRP. The thermal and mechanical loads calculated from [3] and [4] are applied on a single representative weighted-average arc-root radius r_{c_avg} over selected time steps on a CFRP protected by a solid copper foil (SCF). Hypotheses are proposed and subsequently validated for the cohesive behaviour between the SCF and CFRP panel apart from further investigating the effect of a paint layer through parametric study.

1. Introduction

Lightning strike protection (LSP) is necessary to eliminate bulk damage in carbon-fibre reinforced polymer (CFRP) composites which is more detrimental to the residual strength than surface damage in the LSP due to thermal loads. The majority of the current works published on the investigation of the direct effects of a lightning strike (LS) focus on unprotected CFRP panels. They use coupled thermal-electrical based approaches to represent both the loads and the structural damage in CFRP. Among others, two approaches based on the electrical-thermal model of Ogasawara et al. [1] use electrical-thermal analysis to evaluate the effect of resin pyrolysis on the induced bulk damage. Liu et al. [2] considered sophisticated schemes like *Blow-Off-Impulse* (BOI) and Muñoz et al. [3] added pressure-based effects. These successfully demonstrated the effect of rapid thermal loading but did not consider LSP. Moreover, the role of a LSP, especially Solid Copper Foil (SCF) in mitigating the damage otherwise observed in unprotected CFRP has not been explored thoroughly at present. The development of simple and robust models which accurately predict the damage in the LSP and CFRP due to LS is therefore desired. Previous work done in the laboratory proved that the loads applied by the thermally loaded LSP on the first ply of the CFRP panel could be represented by an externally induced pressure because the bulk damage is of mechanical origin. The aim of the present study is to evaluate the effect of the LSP behaviour on the thermal *and* mechanical loads applied onto the first ply, thus enhancing the previous work. A methodology is proposed here to model the LS loads on the SCF as induced thermal-mechanical loads. Additionally, the relatively less numerically explored effects of a paint layer are investigated. The effect of the covering paint layer is emphasised to be represented by an additional corresponding pressure, the magnitude of which is computed so that the rear-face displacement of the combined LSP and CFRP panels coincides with available experimental data. The consideration of LSP and a paint layer in investigative and validation studies is especially justifiable as LSPs, like SCF and Expanded Metal Foil (EMF), have been extensively used in new generation aircraft like the *Airbus A350* and *Boeing 787* for providing protection against LS.

2. Methodology

2.1. Abbreviations and Acronyms

CSDMG	Cohesive Surface Damage (in Abaqus)
Cu	Copper
I	Current
J	Joule heat
P_{acous}	Acoustic pressure
P_{mag}	Magnetic pressure
P_{over}	Overpressure (due to paint)
P_{rad}	Pressure due to thermal radiation
Q_A	Thermal heat flux (anodic)
r	Electrical resistance
r_c	Arc-root radius
r_{c_avg}	Weighted average arc-root radius
σ	Stress
T	Temperature
κ	Thermal conductance

t	Time
u	Rear-face displacement

2.2. Algorithm

The case of reference for the present study is the case of a D current waveform Lightning Strike on a CFRP plate protected by a SCF and covered by a layer of paint described in [14]. The proposed 3D numerical model represents the composite plate with all the plies and the SCF layer as another ply. Decohesions are allowed between all plies. Material models are non-linear. The loading is defined as prescribed pressures and temperatures on the top of the SCF layer. At first time intervals are defined for the loading phases. The evolving surface of current injection at the arc root during the real tests is replaced by fixed surfaces of pressure and temperature injection. The finite element mesh is proposed as a final process of a mesh sensitivity analysis (not presented here). At the end of the simulation, comparisons are made between the numerical results obtained and the experimental results available from the previous studies of [14]. It is shown that the paint can affect drastically the behaviour. The final model proposed here gives the value of the equivalent pressure that could come from this effect on the top of the SCF. The complete simulation process is described on *Figure 1*.

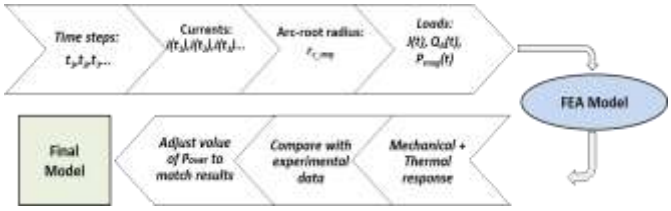

Figure 1 Process map

2.3. Current-Waveform

The D current waveform was considered with the characteristics presented in *Table 1* and calculated by **Erreur ! Source du renvoi introuvable.** [5]

Waveform type	*D*
Amplitude (kA)	100
Rise time (µs)	20

Table 1 Current-waveform characteristics

$$\boldsymbol{I(t) = I_o(e^{-\alpha t} - e^{-\beta t})}\ . \qquad (1)$$

where α=5 $10^4 s^{-1}$ and β=5.2 $10^4 s^{-1}$ and I_o =6.58 $10^6 A$. Values have been taken from reference values of [14].

2.4. Time Steps

Discretised time intervals were proposed at which representative loads were calculated and applied in Abaqus in accordance with the gradient of change of the current with time as presented in *Table 2*. The total time-duration of the current injection was considered to be 75 µs as the majority of the LS direct effects occur in this time-frame [14].

# Time-step	Time (µs)
0	0
1	1
2	5
3	10
4	20
5	27
6	75

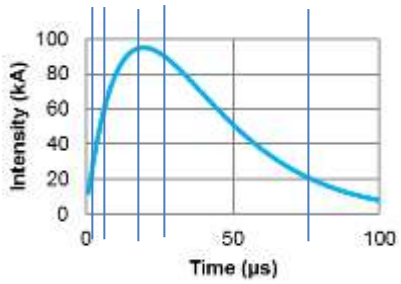

Table 2 Time-steps for load-application

2.5. Arc-root radius

In reality, the arc-root radius r_c of a LS column increases with time and empirical relations are available [4] for its estimation. However, for the sake of modelling simplicity, a single value of the radius r_{c_avg} was hypothesised and estimated for all time-steps, as represented by **Erreur ! Source du renvoi introuvable.**. Evidently, the loads calculated using this hypothesis will differ and will subsequently propose different local results. But from a global perspective, the effects should be the comparable from a qualitative viewpoint.

$$r_{c\_avg} = \frac{\sum_0^n [r_c(t_n) \times I(t_n)]}{\sum_0^n I(t_n)}. \qquad (2)$$

The calculated value of r_{c_avg} is 19.2 mm by considering n = 6 (for a total of 7 time-steps as per *Table 2*). All the subsequently presented loads are calculated using r_{c_avg}.

2.6. Loads

Loads typically associated with a LS are defined as bulk-based or surface-based [6]. It has been concluded previously [6] that in the case of a protected CFRP, the thermal loads are surface-acting and the mechanical loads are relevant to the bulk. Further classification of the loads in terms of *definitive*, *parametric* and *neglected* was proposed. *Definitive* loads are generally well explored in previous literature and their behaviour and effects are emphasized as being known with high confidence. However, *parametric* loads are such that their presence is known to exist, but do not have a consensus on their quantitative effects and mechanisms of interactions. The proposed classification is summarised in *Table 3*.

Type	Definitive	Parametric	Neglected [7] [8]
Thermal/ Surface based	J, Q_A	-	P_{rad}
Mechanical/ Bulk based	P_{mag}	P_{over} *	P_{acous}

* *due to presence of paint layer*

Table 3 Classification of the loads

2.6.1. Thermal Loads

Joule heat *J* was calculated at the time-steps presented in ***Table 2*** by **Erreur ! Source du renvoi introuvable.**.

$$J(t) = \frac{H}{t \times A} = \frac{I(t)^2 \rho l}{A^2}. \qquad (3)$$

where H is the heat generated due to the Joule heating effect and is proportional to the action-integral of the current, $I(t)$ is the current, ρ is the electrical resistivity, l is the thickness of the ply (SCF) and A is the area of the circular strike-zone considering r_{c_avg} as the radius.

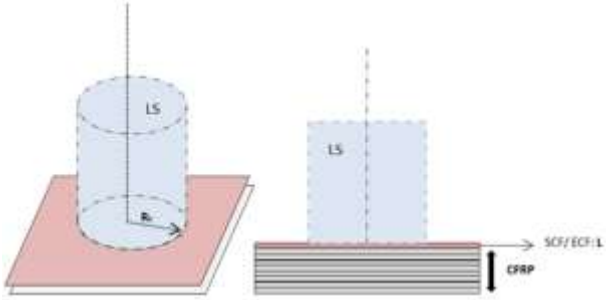

Figure 2 Visualisation of the Joule heat

The current from the LS flows principally through the path of least resistance. Given the extreme difference in the electrical conductivity of Cu and CFRP, it is assumed that the Joule heat occurs only in the SCF. In fact the electrical conductivity of Cu is always three orders of magnitude higher [9] than that of CFRP (longitudinal) from ambient temperature to 3316 °C which is taken as the vaporization temperature of the resin.

Thermal anodic flux Q_A associated with a LS is described by **Erreur ! Source du renvoi introuvable.**.

$$Q_A(t) \approx \frac{10I(t)}{\pi(r_{c\_avg})^2} \qquad (4)$$

2.6.2. Mechanical Loads

Magnetic pressure P_{mag} was calculated using **Erreur ! Source du renvoi introuvable. [3]** to ***Equation 1* [4]*:***

$$P_{panel} = \frac{\mu_0 I^2}{4\pi^2 {r_{c\_avg}}^2} \text{ for } r \le r_{c\_avg} \qquad (5)$$

$$P_{arc} = \frac{\mu_0 I^2}{4\pi^2 r^2} \text{ for } r > r_{c\_avg} \qquad (6)$$

$$P_{mag} = P_{panel} + P_{arc} \qquad (7)$$

Since P_{mag} decay as a function of the radius is quadratic, only the panel contribution of P_{mag} was considered.

Overpressure P_{over} is central to the investigation of the effect of the paint layer which is known to have a detrimental effect on the recorded damage in a protected CFRP [4]. A parametric study was proposed to *tune* and estimate the value of P_{over} by using values ranging from 0 to 50 bars for different durations of the simulation as presented in *Table 4*. The main aim of this exercise was to understand the effect of the paint layer on the response by considering a range of values of equivalent P_{over}. The application of P_{over} during time intervals (*Table 4*) was proposed by trial and error. The reason for applying P_{over} for a finite time duration in the model rather than an impulse was because it was hypothesised (*Figure 3*) that, even after the actual conclusion of the LS, the thermal effects like heat conduction would continue to occur specifically in the SCF, causing the continual heating of the paint in the surrounding regions of the LS zone. This phenomenon contributes to further resin pyrolysis and therefore the prolonged existence and effect of P_{over}.

Cases	*I*	*II*	*III*	*IV*	*V**
0 – 100 µs	50	20	10	7	0
> 100 µs	0	0	4	3	0
	Bars				

**Equivalent to absence of a paint layer*

Table 4 Parametric study of P_{over}

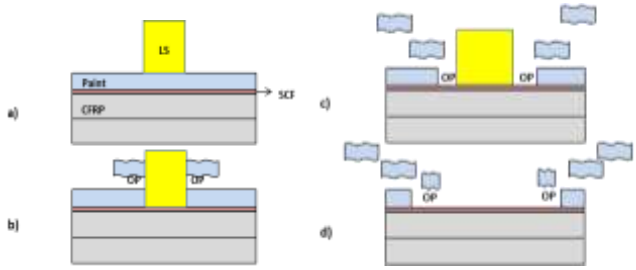

Figure 3 Visualisation of the hypothesis for considering P_{over} in the model; OP ≡ P_{over}

2.7. Materials

Data of T800/M21 were used to model the CFRP. The possible delamination and inter-ply behaviour including the thermal conductance were implemented in Abaqus by using certain interaction properties presented in the Appendix. The mechanism of stress based delamination can be visualised on *Figure 4*.

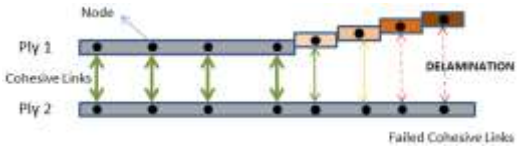

Figure 4 Delamination due to failure of inter-laminar cohesive links

SCF with density of 88 g/m² was used to model the LSP. The *Mie-Grüneisen* equation-of-state (EOS) (*Us-Up* in Abaqus) was used; the input data are presented in *Table 5*.

c_0 (m/s)	s	γ_0
3940	1.49	1.96

Table 5 U_s - U_p EOS parameters (Abaqus) for SCF [10] [11]

The damage and plasticity behaviours for SCF were modelled using the *Johnson-Cook* damage and flow stress models

respectively. The values of the relevant parameters are presented in *Table 6* and *Table 7* respectively.

D_1	D_2	D_3	D_4	D_5	$\dot{\varepsilon}_0$
0.54	4.890	3.03	0.014	1.12	1

Table 6 Johnson-Cook damage parameters for Cu [12]

A	B	C	n	m	$\dot{\varepsilon}_0$
$9\ 10^7$	$2.92\ 10^8$	0.025	0.31	1.09	1

Table 7 Johnson-Cook flow stress parameters for Cu [13]

The other material properties used in the model were from Abdelal et al. [9], such as temperature-dependent specific heat capacities, thermal and electrical conductivities for both CFRP and SCF.

2.8. FEM Model

Abaqus/ Explicit was used to render the model and perform the simulations. The model was meshed with higher refinement in the central region corresponding to the strike-zone to derive results with higher accuracy (Figure 5).

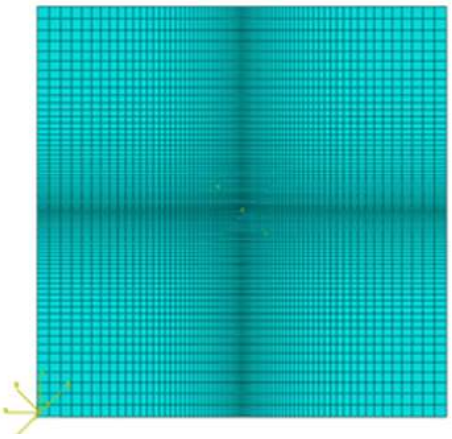

Figure 5 Mesh used in the model with bias (Abaqus)

Panels are 8-ply 330mmx330mm quasi-isotropic T800/M21 plates with stacking-sequence $[45°, 0°, 135°, 90°]_s$. Each CFRP ply is 0.125mm thick whereas the SCF is 0.00986mm thick [14]. Coupled temperature-displacement 3D elements with 8 nodes each were used with designation C3D8T.

Characteristics	CFRP	SCF
#Elements	51200	6400
#Nodes	104976	13122
Bias (half-length)	8	8
#Elements/edge	80	80
Boundary condition	*clamped*	*clamped*

Table 8 Mesh statistics

KI kN/mm^3	*KII* kN/mm^3	*σn* *MPa*	*σs* *MPa*	*GIc* J/m^2	*GIIc* J/m^2	*α*
100	*100*	*50*	*50*	*500*	*1200*	*1.0*

Table 9 Interface specifications

Mechanical *and* thermal **interaction properties** were defined and used in Abaqus for modelling the inter-ply mechanical (possible delamination) and thermal behaviour (heat flow). For the mechanical behaviour, hard frictionless contact and cohesive behaviour were implemented with isotropic stiffness properties in the three principal directions. Further, a quadratic stress criterion was used to enable damage initiation between plies. The damage evolution was implemented with a mixed-mode *Benzeggagh-Kenane* energy criterion for normal and shear loads, apart from including a suitable viscous stabilization coefficient. For the thermal behaviour, thermal conductance of resin of 500 W/m^2K [15] was used to enable heat flow based on an inter-ply clearance criterion. The interaction properties exactly as input into Abaqus are presented in the Appendix.

2.9. Application of Loads

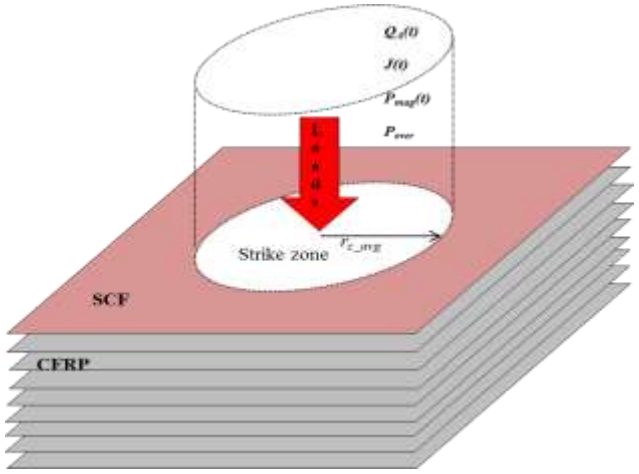

Figure 6 Visualisation of the application of loads in the FEM

It must be noted that the loads has been directly applied on the SCF and not on the paint layer as it is partially ejected because of explosions due to P_{over} as illustrated by *Figure 6*. Thus a separate layer for paint need not be considered in the model which mechanical and thermal properties are neglected. Moreover the paint per se is emphasized to have irrelevant mechanical resistance capabilities for the protection of the CFRP. But as mentioned earlier, and following the same idea as Abdelal et al. [9], the effect of the paint is considered in the proposed analysis by adding its equivalent overpressure P_{over}. A parametric study gives P_{over}.

3. Results

3.1. Effect of SCF-CFRP Interaction

Effect on the Mechanical Behaviour

Different types of cohesive links between the SCF and CFRP were used for the investigation of the dependence of the mechanical response of the protected CFRP on the type of the cohesive link as presented in *Table 10*.

Type	Description
Nominal	Nominal performance of the cohesive links (refer

	Appendix)
Weak	Degraded cohesive links by 1 order of magnitude
Strong	No cohesive link, i.e. SCF and Ply 1 effectively merged
No SCF	Study of the mechanical response of only CFRP

Table 10 Types of SCF-CFRP interactions considered

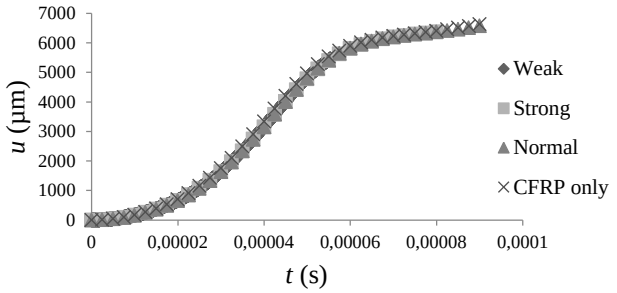

Figure 7 Dependence of rear-face displacements (u) on the SCF-CFRP interaction (mechanical behaviour)

Based on the results presented in *Figure 7*, it is concluded that the choice of the interaction type has negligible effect on the mechanical response of the protected CFRP. Thus future investigation of the mechanical behaviour of the protected CFRP can be pursued by modelling the CFRP alone.

Effect on the Thermal Behaviour

Simulations were performed to assess the effect of the presence or absence of an interaction property between the SCF and CFRP on the thermal response of the protected CFRP. As per *Figure 8*, it can be inferred that the temperature distribution is indeed dependent on the type of interaction. The temperature in the SCF is in the vicinity of 1400 ºC for the case when interaction is considered and 165 ºC for the case without interaction. This needs further investigation in the future based on the temperatures recorded in metals after a LS and research on the parameters defining the thermal conductance in the SCF-CFRP inter-region. Although what is known is that, in reality, the superior thermal properties of Cu enable it to protect the CFRP completely from thermal damage. By this logic, the case which considered the interaction is more acceptable as true as the temperature is near ambient in the CFRP plies below the SCF.

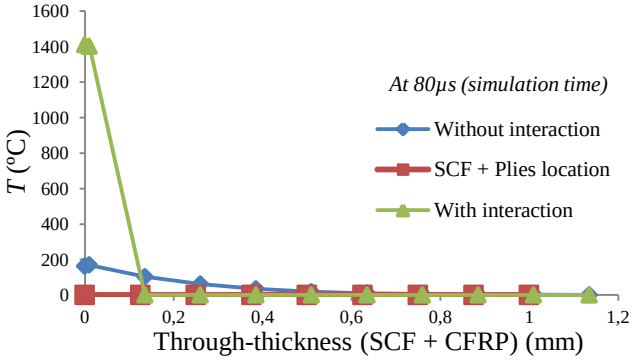

Figure 8 Temperature distributions for SCF + CFRP with and without interactions (thermal behaviour) at 80µs

After performing the simulation for 150 µs, the temperature of the CFRP remained in the vicinity of the ambient temperature suggesting it was in effect unaffected thermally during the relevant duration of the LS (*Figure 9*).

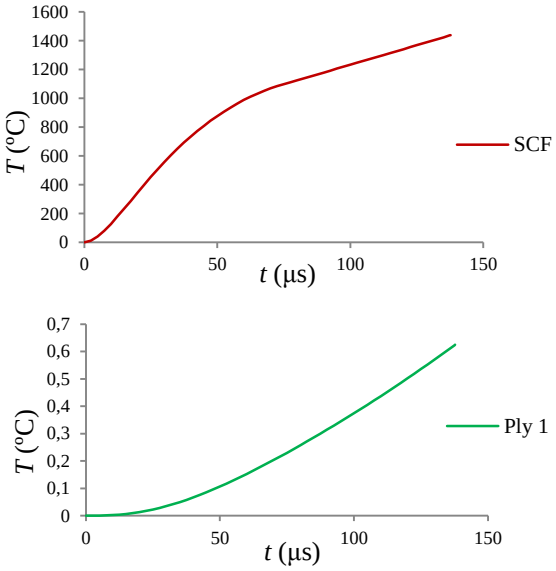

Figure 9 Evolution of temperature with time for SCF (top) and Ply 1 (bottom) considering an interaction property

3.2. Parametric Study of P_{over}

As mentioned previously, inclusion of the effect of the paint is important to represent the real response of a SCF-protected CFRP. *Figure 11* (only available experimental results from Airbus for CFRP protected with SCF) may be compared to *Figure 10* to conclude that the value of P_{over} which best replicates the experimental response is *Case IV* and to a lesser extent *Case III*. In fact it closely matched the qualitative behaviour of Airbus's test campaign *Alder 115* (purple line in *Figure 11*). Possibly more trials with different values of P_{over} with different time duration of application may yield better correspondence in the results quantitatively. Thus further investigation is needed. It is clear that the paint thickness is proportional to the P_{over} as the increased thickness augments the *confinement-effect* of the pyrolised gases of the paint.

It should be noted that the values of the rear-face displacements are found to be higher in the numerical model than the experimental values. This suggests that in this particular case, P_{over} should be less than the pressure load proposed by *Case IV*. This also implies that P_{over} is definitely less than the reported value of 50 bars in published literature [4] but also higher than 0 bars (equivalent to no paint in the model), suggesting that the effect of the paint layer must indeed be taken into account. The parametric study was done without considering the SCF layer as only the mechanical response is being considered (refer *Figure 7*).

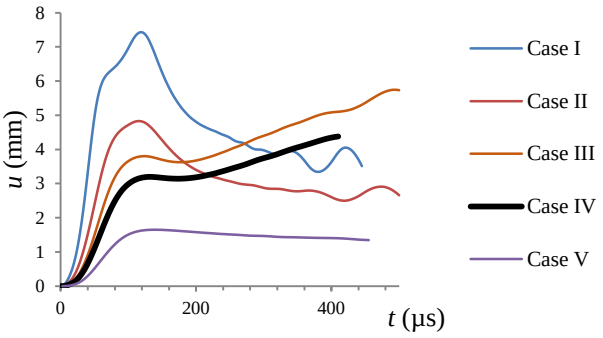

Figure 10 Results of the parametric study of P_{over}; Rear-face displacements (u) for different cases of P_{over}

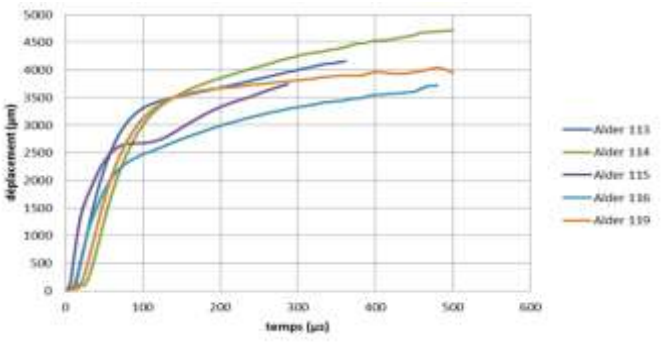

Figure 11 Experimental results for rear-face displacements (u) for SCF protected CFRP (T800/M21); courtesy: Airbus

3.3. Final Proposed Model

The numerical model was first validated for static, dynamic and thermal responses. The final proposed model considered r_{c_avg} and *Case IV* for the values of P_{over}. Selected relevant results are presented in *Table 11*.

No.	Parameter	Units	Value
1	u_{max}	mm	4.38
2	Reserve factors (fibre/ counter-fibre/ in-plane shear)	-	4.4, 5, 3.92
3	Delamination*	mm^2	0
4	T_{max} SCF	ºC	1400 (with interaction)
5	T_{max} 1st Ply	ºC	≈ 0
6	T_{max} 2nd Ply	ºC	0

**CSDMG = 0% (from Abaqus)*

Table 11 Results from the final proposed numerical model

Mechanical Response

In the final proposed model, at 100 µs, the delamination in the CFRP was zero as the Cohesive Surface Damage $CSDMG_{max}$ (Abaqus) reported 0% degradation of the cohesive links. This is consistent with reality and the experimental results; the experimental data from Airbus reported zero delamination as well for a CFRP protected by SCF. A prime conclusion which can be drawn is that the SCF is indeed capable of protecting the inner bulk (CFRP) from structural damage due to delamination. However, the investigation of other types of structural damage in the composite (e.g. fibre-rupture), which can be equally or even more detrimental to the performance of the protected composite, should be considered in further studies.

The mechanical behaviour of models considering other values of P_{over} (as per *Table 4*) was also evaluated. In the model which considered *Case I* of P_{over}, $CSDMG_{max}$ at 100 µs was 30%, suggesting weakening but no delamination. At 500 µs, the reported peak value of CSDMG was 55% but again with no delamination. For the model which considered *Case II* of P_{over}, $CSDMG_{max}$ was 0%, suggesting neither weakening nor delamination. Though at 500 µs, the $CSDMG_{max}$ increased to 10% but again with no delamination for the duration of the LS. Thus it was concluded that even for harsher (i.e. higher) values of P_{over} there is no delamination per se, although there is weakening of structure proportional to the value of the overpressure and the manner of its temporal application in the model.

Thermal Response

The thermal response of the model was not validated as relevant experimental data was unfortunately unavailable for a CFRP protected by SCF. Nevertheless, in the previous section it was demonstrated that when a thermal interaction is considered between SCF and CFRP, temperature in SCF is in the vicinity of 1400 ºC and the temperature in Ply 1 is nearly at ambient temperatures after 80 µs (*Figure 8*). The M21 resin which is used in the CFRP (T800/M21) is claimed to be effective for temperatures up to 150 ºC [16]. As the temperature of CFRP plies is definitely below 150 ºC, according to the numerical model, the CFRP does not undergo any thermal damage. In the SCF, as the temperature was higher as per the numerical model than the $T_{melting}$ of Cu i.e. 1085 ºC, there would be consequential material damage in the SCF, as corroborated by experiments and actual events. As the priority is the protection of the bulk i.e. CFRP from thermal damage, the results are considered to be sensible and qualitatively representative of the phenomena and effects.

Stress Validation of CFRP

A stress validation study was performed to confirm the absence of material damage in the CFRP by analysing the principle stress values and comparing them with available values from the manufacturer. From *Table 12*, it was concluded that there was no material damage in the CFRP.

σ (MPa)	Abaqus	Manufacturer's claims [17]	Reserve factor
$\sigma_{11\ max}$	830.4 *(in Ply 8)*	2650	4.4
$\sigma_{22\ max}$	-422.6 *(in Ply 1)*	1570	5
$\tau_{12\ max}$	28.8 *(in Ply 1)*	98	3.92

Table 12 Stress comparison of the numerical model with published values of T800/M21

4. Conclusion

A novel coupled thermal-mechanical model was proposed to investigate and estimate the effect of a LS on a CFRP panel protected by a SCF after considering the relevant loads associated with a LS. It was concluded that the SCF is able to completely protect CFRP from bulk related damage like delamination, although with the possibility of material damage in the SCF in the surface. As there was qualitative correlation of the numerical results with the available experimental data from Airbus, the hypothesis of using a weighted-average arc-root radius and using the Joule heat generated in the SCF exclusively is concluded to be justifiable. It was also concluded that the SCF is more relevant for the thermal effects while the CFRP alone is more relevant for the mechanical response in a SCF-protected CFRP. Lastly, the effect of a paint layer was investigated and its equivalent value and duration of application of overpressure P_{over} was estimated.

Acknowledgements

This work contributed to a master's thesis for an ongoing project undertaken by *ISAE-Supaero*, *Institut Clément Ader* (ICA) and *Airbus Group Innovations* (AGI), France. Thanks to M.D. Wilson for assisting with the editing and improving the linguistic clarity of this work.

References

[1] T. Ogasawara, Y. Hirano and A. Yoshimora, "Coupled thermal-electrical analysis for carbon fiber/ epoxy composites exposed to simulated lightning current," *Composite Part A: Applied Science and Manufacturing,* vol. 41.8, pp. 973-981, 2010.

[2] Z. Q. Liu, Z. F. Yue, F.S. Wang and Y.Y. Ji, "Combining Analysis of Coupled Electrical-Thermal and BLOW-OFF Impulse Effects on Composite laminate Induced by Lightning Strike," *Applied Composite Materials,* vol. 22.2, pp. 189-207, 2015.

[3] R. Muñoz, S. Delgado, C. González, B. López-Romano, D.Y. Wang and J. Llorca, "Modeling Lightning Impact Thermo-Mechanical Damage on Composite Materials," *Applied Composite Materials,* vol. 21.1, pp. 149-164, 2014.

[4] L. Chemartin and P. Lalande, B. Peyrou, A. Chazottes, P.Q. Elias, C. Delalondre, B.G. Cheron and F. Lago, "Direct effects of lightning on aircraft structure: analysis of the thermal, electrical and mechanical constraints," *Aerospace Lab, issue 5, AL05-09,* 2012.

[5] J. Parmantier, F. Issac and V. Gobon, "Indirect Effects of Lightning on Aircraft and Rotorcraft," *Aerospace Lab Journal,* vol. Issue 5, AL05-10, 2012.

[6] B. Lepetit, F. Soulas, S. Guinard, I. Revel, G. Peres and Y. Duval, "Analysis of composite panel damages due to a lightning strike: mechanical effects," *ICOLSE 2013,* Seattle, 2013.

[7] B. Kumar, R. Singh and T. Nakamura, "Degradation of Carbon Fiber-reinforced Epoxy Composites by Ultraviolet Radiation and Condensation," *Journal of Composite Materials,* vol. 36, no. 24, 2002.

[8] E. Rupke, "Lightning Direct Efftects Handbook," Lightning Technologies Inc., Rept. AGATE-WP3.1-031027-043, Pittsfield, MA, 1 March 2002. [Online]. Available: http://www.niar.wichita.edu/agate/documents/lightning/wp3.1-031027-043.pdf.

[9] G. Abdelal and A. Murphy, "Nonlinear numerical modelling of lightning strike effect on composite panels with temperature dependent material properties," *Composite Structures,* vol. 109, pp. 268-278, 2014.

[10] A. Mitchell and W. Nellis, "Shock compression of aluminium, copper, and tantalum," *Journal of Applied Physics,* vol. 52, no. 5, 1981.

[11] R. MacDonald and W. MacDonald, "Thermodynamic properties of fcc metals at high temperatures," *Physical Review B,* vol. 24, no. 4, 1981.

[12] C. Rao, V. Narayanamurthy and K. Simha, in *Applied Impact Mechanics*, John Wiley & Sons, 2016, p. 159.

[13] M. Meyers, in *Dynamic Behavior of Materials*, New York, John Wiley & Sons, DOI: 10.1002/9780470172278 1994.

[14] F. Soulas, *Development of a lightning strike mechanical model for the prediction of damage of aeronautical composite panels,* Université de Toulouse, 2016 (PhD Thesis).

[15] S. Mirmira, M. Jackson and L. Fletcher, "Effective thermal conductivity and thermal contact conductance of graphite fiber composites," *Journal of Thermophysics and Heat Transfer,* vol. 15, pp. 18-26, 2001.

[16] Hexcel, "M21 Properties," [Online]. Available: http://www.hexcel.com/Resources/DataSheets/Prepreg-Data-Sheets/M21_global.pdf.

[17] Toray, "Toray 800," [Online]. Available: http://www.toraycfa.com/pdfs/T800HDataSheet.pdf.

[18] Y. Li, R. Li, L. Lu and X. Huang, "Experimental study of damage characteristics of carbon woven fabric/ epoxy laminates subjected to lightning strike," *Composites Part A: Applied Science and Manufacturing,* vol. 79, pp. 164-175, 2015.

[19] F. Soulas, C. Espinosa and F. Lachaud, S. Guinard, B. Lepetit and I. Revel"Equivalent impact set-up for lightning strike damage on composite coupons," in *20th International Conference on Composite Materials* , Copenhagen, 2015.

[20] R. Ranjith, R. Myong and S. Lee, "Computational Investigation of Lightning Strike Effects on Aircraft Components," *International Journal of Aeronautical and Space Sciences,* vol. 15.1, pp. 44-53, 2014.

[21] E. Etemadi, J. Zamani, A. Francesconi, M. Mousavi and C. Giacomuzzo, "A New Set-Up to Investigate Plastic Deformation of Face Centered Cubic Metals in High Strain Rate Loading," *Modern Applied Science,* vol. 8.2,

pp. 94-106, 2014.

[22] D. Morgan, C. Hardwick, S. Haigh and A. Meakins, "The Interaction of Lightning with Aircraft and the Challenges of Lightning Testing," *Aerospace Lab (Onera)*, 2012.

[23] F. Report, "Investigation of the parameters affecting mechanical forces in aluminium and CFC plates subject to simulated lightning strikes," Transport Research & Technological Development Program, 1997.

[24] Tiwari, N; NPTEL, "Introduction to Composite Materials and Structures," [Online]. Available: http://nptel.ac.in/courses/112104168/L32.pdf.

[25] "Section 3: Progressive Ply Failure and Delamination Modelling," February 2002. [Online]. Available: http://pages.mscsoftware.com/rs/mscsoftware/images/Sec3_Progressive_failure_and _delam_021712.pdf.

[26] flightsafety.org, "ASN Aircraft Accident Boeing 707-102 N709PA," [Online]. Available: http://aviation-safety.net/database/record.php?id=19631208-0.

[27] Lord, "UltraConductive™ Film and Coatings for Lightning Strike Protection and EMI Shielding," [Online]. Available: http://www.lord.com/products-and-solutions/brands/ultraconductive.

[28] Dexmet Corporation, "MicroGrid® Precision Expanded Metal and Metal Foil," [Online]. Available: http://www.dexmet.com/products/expanded-metals/.

[29] S. Haigh, "Impulse Effects during Simulated Lightning Attachments to Lightweight Composite Panels," in *International Conference on Lightning and Static Electricity*, Paris, 2007.

[30] M.A. Zocher and P.J. Mauldin, "An evaluation of several hardening models using Taylor cylinder impact data," in Conference *Computational Methods in Applied Sciences and Engineering*, Barcelona, 2000.

[31] A. Banerjee, S. Dhar, S. Acharya, D. Datta and N. Nayak, "Determination of Johnson Cook material failure model constants and numerical modelling of Charpy impact test of armour steel," Material Science & Engineering A, vol. 640, pp. 200-209, 2015.

[32] D. Betts, A. Salo, C. Bowen and H. Kim, "Characterisation and modelling of the cured shapes of arbitrary layup bistable composite laminates," *Elsevier: Composite Structures*, vol. 92, p. 1696, 2009.

[33] A. Uguen, L. Zubillaga, A. Turon and N. Carrère, "Comparison of cohesive zone models used to predict delamination initiated from free-edges: validation against experimental results," in *ECCM - 16th European Conference on Composite Materials*, Seville, 2014.

[34] G. Johnson and W. Cook, "A constitutive model and data for metals subjected to large strains, high strain rates and high temperatures," in *Proceedings of the 7th International Symposium on Ballistics*, 1983.

Appendix

Mechanical: *Int_prop_1:* General contact properties

Tangential behaviour	Frictionless
Normal behaviour	Pressure over-closure: Hard contact Constraint enforcement method: Default Separation after contact: Selected

Mechanical: *Int_prop_2*: Cohesive behaviour and damage criteria used [14]

<table>
<tr><td>Cohesive Behaviour</td><td>• Eligibility of Slave Nodes: Any slave node experiencing contact
• Use of uncoupled stiffness coefficients
<table><tr><td>K_{nn}</td><td>K_{ss}</td><td>K_{tt}</td></tr><tr><td>$1x10^{14}$</td><td>$1x10^{14}$</td><td>$1x10^{14}$</td></tr></table></td></tr>
<tr><td colspan="2">Damage
<table>
<tr><td>Initiation</td><td>Criterion: Quadratic traction
<table><tr><td>Normal Only</td><td>Shear -1 Only</td><td>Shear -2 Only</td></tr><tr><td>$6x10^7$</td><td>$6x10^7$</td><td>$6x10^7$</td></tr></table></td></tr>
<tr><td>Evolution</td><td>Type: Energy
Softening: Linear
Mixed mode behaviour: Benzeggagh-Kenane
Mode mix ratio: Energy
BK Exponent: 1
<table><tr><td>Normal Fracture Energy (J)</td><td>1st Shear Fracture Energy (J)</td><td>2nd Shear Fracture Energy (J)</td></tr><tr><td>500</td><td>1000</td><td>1000</td></tr></table></td></tr>
<tr><td>Stabilisation</td><td>Viscosity coefficient: 1E-7 Pa. s</td></tr>
</table></td></tr>
</table>

Thermal: *Int-prop_3*: Inter-ply conductance of 500 W/m^2K [15] based on an inter-ply clearance criterion.